Mathematical modelling and experimental validation of electrostatic sensors for rotational speed measurement

Mathematical modelling and experimental validation of electrostatic sensors for rotational speed measurement

Lijuan Wang[1,2] and Yong Yan[2]

[1] School of Control and Computer Engineering, North China Electric Power University, Beijing 102206, People's Republic of China
[2] School of Engineering and Digital Arts, University of Kent, Canterbury, Kent CT2 7NT, UK

E-mail: y.yan@kent.ac.uk

Abstract

Recent research has demonstrated that electrostatic sensors can be applied to the measurement of rotational speed with excellent repeatability and accuracy under a range of conditions. However, the sensing mechanism and fundamental characteristics of the electrostatic sensors are still largely unknown and hence the design of the sensors is not optimised for rotational speed measurement. This paper presents the mathematical modelling of strip electrostatic sensors for rotational speed measurement and associated experimental studies for the validation of the modelling results. In the modelling, an ideal point charge on the surface of the rotating object is regarded as an impulse input to the sensing system. The fundamental characteristics of the sensor, including spatial sensitivity, spatial filtering length and signal bandwidth, are quantified from the developed model. The effects of the geometric dimensions of the electrode, the distance between the electrode and the rotor surface and the rotational speed being measured on the performance of the sensor are analyzed. A close agreement between the modelling results and experimental measurements has been observed under a range of conditions. Optimal design of the electrostatic sensor for a given rotor size is suggested and discussed in accordance with the modelling and experimental results.

Keywords: rotational speed measurement, electrostatic sensors, mathematical modelling, spatial sensitivity, spatial filtering, bandwidth

(Some figures may appear in colour only in the online journal)

Nomenclature

B	Effective signal bandwidth
D	Diameter of the rotor; also diameter of the circular trajectory of the point charge P
f_c	Cut-off frequency of the sensor
f_{max}	Maximum frequency of the signal from the sensor
h_s	Impulse response of the sensor
I_s	Current output of the sensor
K	Proportionality coefficient
L	Length of the electrode
n	Rotational speed of the point charge (rpm, revolutions per minute)
O	Origin of the plan XOY
O′	Origin of the projected plan X′O′Y′
O″	Centre of trajectory of the mirrored point charge
P	An ideal point charge
$P′$	Mirrored point charge of P
Q	A given point which is located on the right-hand side of Y=v plane
q	Electric quantity of the point charge
$q′$	Induced charge on the electrode

R_{hh}	Autocorrelation function of the impulse response h_s
S	The shortest distance between the electrode surface and the circular trajectory of the point charge
S_h	Power spectrum of the impulse response h_s
S_s	Spatial sensitivity of the sensor
$S'(t)$	Signal from the electrostatic sensor
$\bar{S}$	Mean value of $S(t)$
$S'(t)$	Normalised signal $S(t)$
S_{max}	Maximum value of $S(t)$
u, m, r	Coordinates of point Q in X, Y and Z axes
V	Electric potential
v	Location of the electrode on Y-axis
W	Width of the electrode
W_e	Spatial filtering length of the sensor
x, y, z	Coordinates of the ideal point charge P in X, Y and Z axes
β_i	A symbol function
δ_L	L normalised to D
δ_S	S normalised to D
δ_W	W normalised to D
δ_{W_e}	W_e normalised to D
δ_x	x normalised to D
δ_y	y normalised to D
δ_z	z normalised to D
ε	Permittivity of the medium in which the point charge exists
θ	Rotational angle of the ideal point charge
τ	Time corresponding to the two peaks of the impulse response h_s with reference to the origin
τ_e	Time difference between the two peaks of the impulse response h_s
φ_e	Central angle taken by the rotor rotating over W_e
ω	Angular speed of the point charge

1. Introduction

Rotational speed measurement through electrostatic sensing and signal processing techniques has been reported recently [1]. The sensing principle is based on the phenomena of triboelectric charging of the rotor surface in rotational motion and electrostatic induction of the rotor surface on the electrode of the sensor. An electrostatic sensor array evenly mounted around the rotor surface is used to acquire signals for the rotational measurements [1]. A simpler method is to use a single or double electrode to sense the rotational movement of a rotor [2, 3]. In comparison with existing tachometers based on optical, electrical, magnetic and imaging techniques [4–6], the electrostatic sensing-based rotational speed measurement technique has advantages of noncontact measurement, low cost and suitability for hostile environments. Since the electrostatic sensors have no direct contact with the rotor, there is no wear problem that adversely affects some of the existing techniques such as mechanical tachometers. The electrostatic sensors have no requirement for the fitting of an opaque disc on the rotor, which is an essential element of photoelectric tachometers. The presence of dust around the rotor can affect the operation of optical tachometers, but has little impact on the electrostatic sensors.

Meanwhile, the structural simplicity, low cost and robustness of the electrostatic sensors make the technique suitable for a wider range of industrial applications. Moreover, the flexibility in the arrangement of a variable number of electrostatic sensors around the rotor [1–3] allows the accurate rotational speed measurement for different sized rotors and this is a significant advantage over mechanical and stroboscopic tachometers.

Recent research on electrostatic sensing-based rotational speed measurement is concentrated on the performance assessment of the measurement system [1–3]. There is a lack of research into the in-depth understanding of the sensing mechanism and fundamental characteristics of the electrostatic sensors for rotational speed measurement. In recent years, different modelling work on the electrostatic sensors in different shapes for the flow measurement of pneumatically conveyed particles has been conducted to understand the mechanism of the interaction between the electrostatic sensors and the target object being measured. Applying the theory of electrical coupling, Gajewski [7] proposed a model with two point charges flowing one after another and rectilinearly along the geometrical axis of a metal-ring probe and obtained the voltage drop across the impedance of a measuring system consisting of the probe and measuring device. In their later modelling work, the metal-ring probe was separated from the flow of charged solid particles by a fragment of a dielectric pipe on which the ring was mounted and a two-charged-body system (a point charge and a charged metal-ring probe) was proposed [8]. The point charge was then replaced by a charged solid-particle column travelling in a pipe and hence a three-electrode system (a net electric charge, a ring probe and a grounded electromagnetic screen) was implemented to find the relationships between the space charge density or net charge and the probe potential [9]. Yan et al [10] developed simplified physical and mathematical models of the ring-shaped electrostatic sensor by studying the impulse response to a point charge moving through the electrode and established the relationship between the current output of the sensor and the point charge. The spatial sensitivity, spatial filtering effect and frequency response of the sensor were analyzed together with their effects on particle velocity measurement accuracy. Murnane et al [11] described the model of a square-shaped electrode by applying an electrostatic mirror imaging approach and determined the distribution of charge density on the electrode as the variation of the point charge position. Peng et al [12] also developed the simplified physical and mathematical models of a square-shaped electrostatic sensor in pneumatic pipelines, identified the sensitivity distribution and frequency response of the sensor and investigated effects of the geometric dimensions and attributes of charged particles on the characteristics of the sensor. Krabicka et al [13, 14] compared the ring- and rod-shaped electrodes through finite element modelling and addressed the optimization of intrusive electrostatic sensors in terms of electrode dimensions and intrusion depth. Through finite element analysis, Xu et al [15] investigated the sensing characteristics of ring-shaped electrostatic inductive sensors for the flow parameter measurement of pneumatically conveyed particles. In a similar way, they also studied the arc-shaped electrostatic sensor arrays through computational modelling and practical experimentation [16]. Zhang et al [17, 18] also used the finite element method to analyze the spatial sensitivity
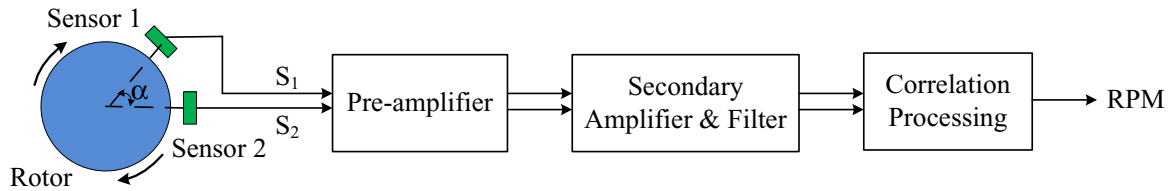
Figure 1. Principle of the speed measurement system using dual sensors.

of the ring-shaped electrostatic sensor in the time and frequency domains, aiming to improve its performance and to achieve uniform spatial sensitivity. Most recently, a 3D mathematical model of a linear electrostatic sensor array is presented by Xu *et al* [19] to determine the filtering characteristics and spatial selectivity of the array.

In the previous modelling work as outlined above, the targets to be measured are all charged particles in linear motion regardless of the shape of the electrode (ring, arc, square or rod). However, there has been no reported work on the modelling and characterisation of strip-type electrodes for rotational speed measurement systems. Consequently, this paper is concerned with the mathematical modelling of strip electrostatic sensors, analysis of their sensing properties and their optimised design for rotational speed measurement. During rotational motion, electrostatic charge is produced on the rotor surface and the quantity of charge depends on many factors, including the material type, surface roughness and speed of the rotor as well as the environmental conditions such as relative humidity and temperature. However, it is difficult to quantify the relationship between the quantity and distribution of the charge and the influencing factors. Moreover, the electric field resulting from the interaction between the source charge and the induced charge is rather complex. Consequently, the mathematical modelling is established based on an ideal point charge and the method of images. The point charge can be considered as an infinite element on the charged surface of the rotor. When rotating over the electrode, the point charge can be regarded as an impulse input to the sensing system and then the system yields current output. Based on the developed model, current output, spatial sensitivity, spatial filtering length and signal bandwidth of the sensor are quantified respectively through analytical modelling and numerical simulation. Moreover, the effects of physical parameters of the sensor on the performance of the measurement system are analyzed to obtain the optimised design of the sensor. Experimental tests are conducted on a purpose-built test rig to validate the modelling results.

2. Modelling of strip electrostatic sensors

2.1. Principle of the rotational speed measurement based on electrostatic sensors

Since the principle of the rotational speed measurement based on electrostatic sensing and correlation signal processing has been described elsewhere [1–3], only a brief description is given here for the convenience of the reader. During the continuous process of rotating motion, electric charges are produced and accumulated on the rotor surface due to the friction between the rotor surface and air. The electric charge on the rotor surface can be detected using electrostatic sensors coupled with

suitable signal conditioning and processing circuits. Recent research has used a single sensor, dual sensors and multi-sensors around the rotor [1–3]. Figure 1 shows the principle of the speed measurement system using dual electrostatic sensors. For the system given in figure 1, the rotational speed in RPM (revolutions per minute) of the rotor is calculated from:

$$\text{RPM} = \frac{30\alpha}{\pi\tau} \tag{1}$$

where α is the angular separation between the sensors (figure 1), τ is the transit time taken by the rotor to rotate from Sensor 1 to Sensor 2, which is determined through cross-correlation between the two electrostatic signals S_1 and S_2 [1]. The rotational speed can also be measured using a single sensor [3], quadruple sensors [1] or more sensors.

2.2. Physical model of the electrostatic sensor

The physical model of the sensing system for rotational speed measurement consists of a rotor to be measured, a strip-shaped electrode and associated signal conditioning and processing circuits, as shown in figure 2(*a*). Figure 2(*b*) shows the simplified model of the sensing system. Because the charged rotor surface can be considered as the superposition of numerous point charges, a single point charge is introduced in the model. The electrode is regarded as a perfectly conductive strip connected to the electronics with input resistance R_i. In this study, only strip electrodes are considered in view of the fact that the electrodes are part of a printed circuit board as part of the signal conditioning and processing unit [1], though the electrodes in other more complex geometrical shapes, such a curved strip, are possible in principle. The point charge rotating along a circle with a diameter of the rotor is equivalent to an impulsive input to the sensing system and thus the impulse response can be used to determine the characteristics of the sensor. The electric field pattern due to a positive point charge is shown in figure 2(*b*), in the vicinity of the electrode.

2.3. Mathematical model of the electrostatic sensor

To simplify calculations and visualize the distribution of the electric field due to the interaction between a source charge and conducting surface, the method of images together with theories of electrostatics are applied to the mathematical modelling of the electrostatic sensor. The validity of the method of images rests upon a corollary of the uniqueness theorem [20]. That is to say, the method is based on the fact that the tangential component of the electrical field on the surface of a conductor is zero whilst the electric field strength in a region is uniquely defined by its normal component over the surface that confines that region.
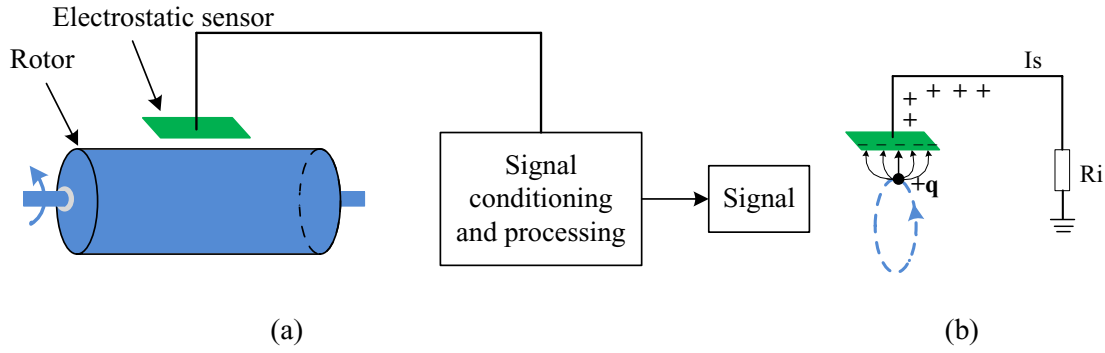
Figure 2. Physical and simplified models of the sensing system for rotational speed measurement. (*a*) Physical model of the sensing system. (*b*) Simplified model of the sensing system.
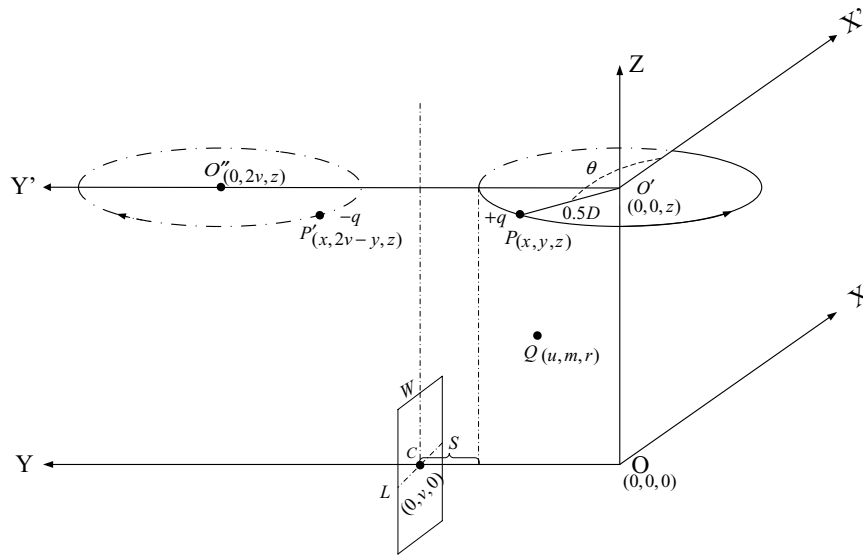

Figure 3. Mathematical model of a strip electrostatic sensor for rotational speed measurement.

In the rotational speed measurement system, an ideal point charge as the infinite element on the charged rotor surface is assumed to rotate along a circular trajectory. A strip electrode placed at the midpoint between the source charge and the mirror charge can be considered as a zero-potential plane, which corresponds to the uniqueness theorem. In this case, the electrode, though electrically insulated and connected to a signal conditioning circuit, is part of the zero-potential plane. The mathematical model of a strip electrostatic sensor for rotational speed measurement is shown in figure 3. This model is established with the following assumptions:

(a) An ideal point charge (*P*) with the electric quantity of $+q$ is rotating at an angular speed (ω) on a certain plan (X′O′Y′) parallel to the basic plan (XOY). The diameter of the circular trajectory is *D*.

(b) The geometric dimensions of the strip electrostatic electrode are *W*-width, *L*-length and zero-thickness. *W* and *L* are infinite length. The electric potential of the electrode is 0.

(c) The electrostatic sensor is placed perpendicular to the Y-axis and its centre is located on the Y-axis. The distance between the electrode and the rotating trajectory is *S*.

(d) *P′* is the mirrored charge of the ideal point charge (*P*). *P* and *P′* have the equal magnitude of charge but opposite polarities.

In the electric field generated by *P* and *P′*, the potential *V* of a given point $Q(u, m, r)$ which is located on the right side of Y = *v* plane is represented by

$$V = \frac{1}{4\pi\varepsilon}\left(\frac{q}{\sqrt{(x-u)^2 + (v-y)^2 + (z-r)^2}} \right.$$

$$\left. + \frac{-q}{\sqrt{(x-u)^2 + (2v-y-m)^2 + (z-r)^2}} \right) \quad (2)$$

where ε is the permittivity of the medium in which the point charge exists. *x*, *y*, *z*, *u*, *v*, *r* and *m* are the coordinate values of the points shown in figure 3. When *m* is equal to *v*, thus *V* is zero which conforms to the assumptions.

Charge density σ on the surface of the electrode is given by

$$\sigma = -\varepsilon \frac{\partial V}{\partial y}\bigg|_{m=v} = \frac{-q(v-y)}{2\pi[(u-x)^2 + (v-y)^2 + (z-r)^2]^{3/2}} \quad (3)$$

So, the total induced charge q' on the electrode surface is determined from

$$q' = \int_{-L/2}^{L/2} \int_{-W/2}^{W/2} \sigma \, \mathrm{d}u \, \mathrm{d}r$$

$$= -\frac{q}{2\pi} \int_{-L/2}^{L/2} \int_{-W/2}^{W/2} \frac{v - y}{[(u-x)^2 + (v-y)^2 + (z-r)^2]^{3/2}} \, \mathrm{d}u \, \mathrm{d}r \tag{4}$$

where

$$v = 0.5D + S, \quad x = 0.5D \cos\theta, \quad y = 0.5D \sin\theta \tag{5}$$

θ is the central angle that the point charge passed by.

Substituting equation (5) into equation (4) yields

$$q' = -\frac{q}{2\pi} \int_{-L/2}^{L/2} \int_{-W/2}^{W/2} \frac{0.5D + S - 0.5D \sin\theta}{\begin{bmatrix} (u - 0.5D\cos\theta)^2 \\ + (0.5D + S - 0.5D\sin\theta)^2 \\ + (z-r)^2 \end{bmatrix}^{3/2}} \, \mathrm{d}u \, \mathrm{d}r \tag{6}$$

Since $\theta = \omega t$, equation (4) can be rewritten as

$$q' = -\frac{q}{2\pi} \int_{-L/2}^{L/2} \int_{-W/2}^{W/2} \frac{0.5D + S - 0.5D\sin(\omega t)}{\begin{bmatrix} (u - 0.5D\cos(\omega t))^2 \\ + (0.5D + S - 0.5D\sin(\omega t))^2 \\ + (z-r)^2 \end{bmatrix}^{3/2}} \, \mathrm{d}u \, \mathrm{d}r \tag{7}$$

The actual current output $I_s(t)$ of the sensor due to the movement of the point charge along the circular trajectory is given by

$$I_s(t) = \frac{\mathrm{d}q'}{\mathrm{d}t} \tag{8}$$

A point charge approaching to the electrode along a circular trajectory from infinity is equivalent to an impulse input with amplitude q to the sensing system, thus the impulse response $h_s(t)$ of the system is given by

$$h_s(t) = \frac{I_s(t)}{q} = \frac{1}{q} \frac{\mathrm{d}q'}{\mathrm{d}t} \tag{9}$$

Equation (7) implies that, for a point charge in rotational motion, the sensor output depends on factors including geometric dimensions of the electrode (W and L), diameter of the circular trajectory of the point charge (D), angular speed (ω), distance between the electrode surface and the circular trajectory (S) and the height of the point charge located in space (z). Figure 4 shows a typical example of the induced charge on the sensor and corresponding waveform of the sensor output, when the rotational speed is constant.

3. Sensing characteristics

3.1. Spatial sensitivity

The model of the electrostatic sensor indicates that the sensor output depends on the location of the point charge for a given electrostatic sensor. The spatial sensitivity S_s can be defined as
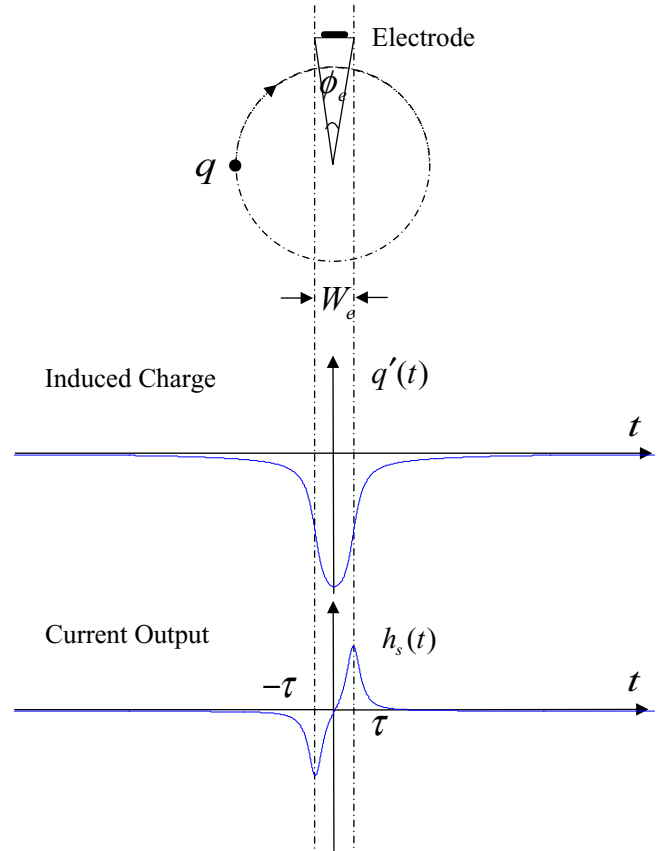

Figure 4. A typical example of the induced charge on the electrode and corresponding waveform of the sensor output.

$$S_s(x, y, z) = \left| \frac{q'(x, y, z)}{q} \right| \tag{10}$$

Taking D as the basic dimensional unit in the sensing system, W, L, S, x, y and z can all be normalised with reference to D and hence become dimensionless parameters, i.e. δ_W, δ_L, δ_S, δ_x, δ_y and δ_z, respectively,

$$\delta_W = \frac{W}{D}, \quad \delta_L = \frac{L}{D}, \quad \delta_S = \frac{S}{D},$$
$$\delta_x = \frac{x}{D} = 0.5\cos\theta, \quad \delta_y = \frac{y}{D} = 0.5\sin\theta \tag{11}$$
$$\delta_z = \frac{z}{D}.$$

Substituting all the dimensionless parameters into equation (10), the spatial sensitivity becomes

$$S_s(\theta, \delta_z) = \frac{1}{4\pi}$$
$$\times \sum_{i=1}^{4} \arctan \frac{(0.5\delta_W + 0.5\beta_i\cos\theta)(0.5\delta_L + (-1)^i\delta_z)}{(0.5 + \delta_S - 0.5\sin\theta) \sqrt{\begin{array}{l} (0.5 + \delta_S - 0.5\sin\theta)^2 \\ + (0.5\delta_W + 0.5\beta_i\cos\theta)^2 \\ + (0.5\delta_L + (-1)^i\delta_z)^2 \end{array}}} \tag{12}$$

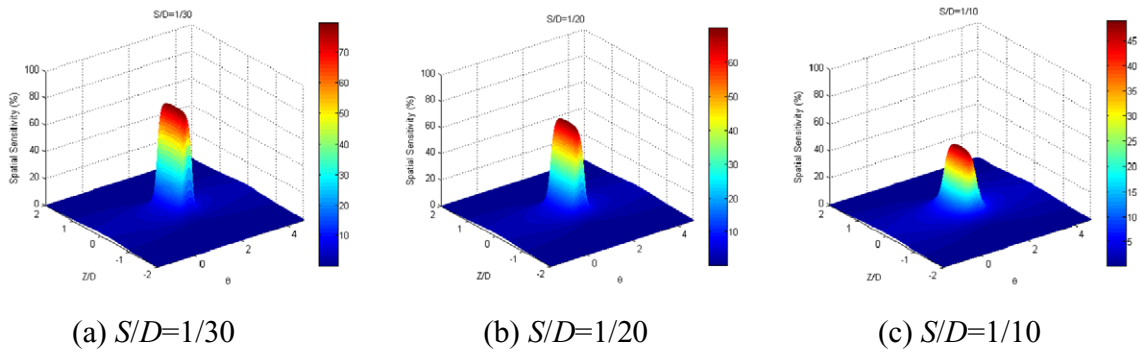where $\beta_i = \mathrm{sgn}(i - 2.5)$.

Figure 5. Spatial sensitivity of the electrostatic sensor for variable *S/D*: (*a*) *S/D* = 1/30, (*b*) *S/D* = 1/20, (*c*) *S/D* = 1/10.
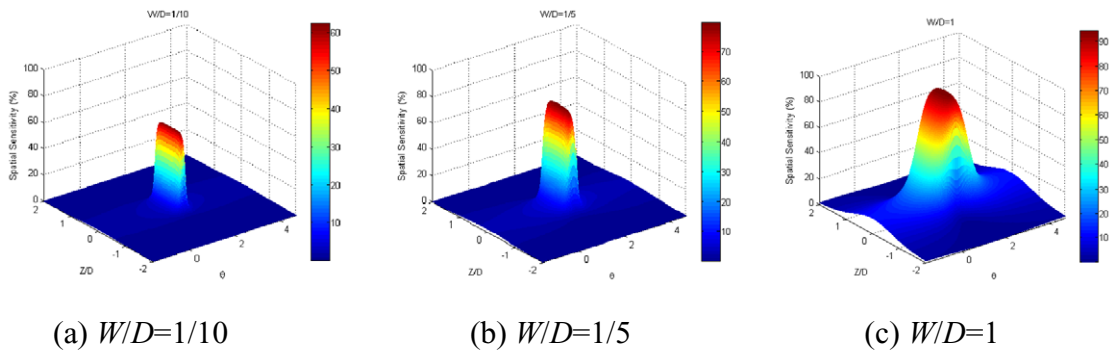

Figure 6. Spatial sensitivity of the electrostatic sensor for variable *W/D*: (*a*) *W/D* = 1/10, (*b*) *W/D* = 1/5, (*c*) *W/D* = 1.
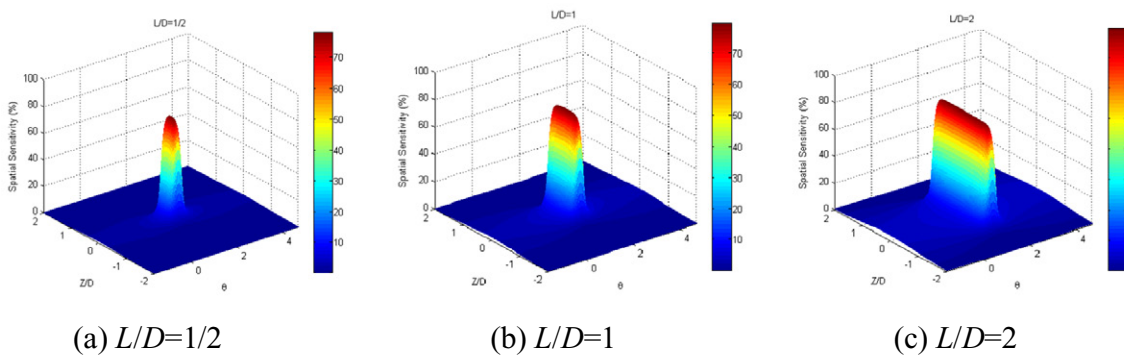

Figure 7. Spatial sensitivity of the electrostatic sensor for variable *L/D*: (*a*) *L/D* = 1/2, (*b*) *L/D* = 1, (*c*) *L/D* = 2.

From equation (12) we can see the spatial sensitivity of the sensor in a given location (θ, δ_z) is determined by the shortest distance between the circular trajectory and the electrode (*S*) and the geometric dimensions of the electrode (*W* and *L*). For each of the three parameters, three realistic, representative cases are considered in this study: *S/D* = 1/30, 1/20, 1/10; *W/D* = 1/10, 1/5, 1 and *L/D* = 1/2, 1, 2.

Substituting δ_W = 1/5 and δ_L = 1 to equation (12), the effects of the distance (*S*) between the electrode and the surface of the rotor on the spatial sensitivity of the sensor are illustrated in figure 5. The spatial sensitivity decreases with δ_S = *S/D* because the farther the distance between the electrode and the rotor surface, the less the induced charge that is yielded on the electrode. Moreover, δ_S affects significantly the maximum sensitivity, which reduces from 80% to 50% as δ_S increases

from 1/30 to 1/10. At the region far away from *z* = 0, the variation in spatial sensitivity is insignificant due to the limited geometric dimensions of the electrode.

In the case that δ_L = 1 and δ_S = 1/30, the effect of the electrode width (*W*) on the spatial sensitivity is obtained and shown in figure 6. It is evident that the overall sensitivity of the sensor increases with δ_W, particularly in the region away from the geometric center of the electrode. This phenomenon is due to more sensing area for a rotating charge when the width of electrode becomes larger.

δ_W and δ_S are set to 1/5 and 1/30 respectively in order to investigate how the length of the electrode (*L*) affects the spatial sensitivity of the sensor. Figure 7 illustrates the spatial sensitivity for variable δ_L = *L/D*. As expected, δ_L affects primarily the axial distribution of the sensitivity, that is, the

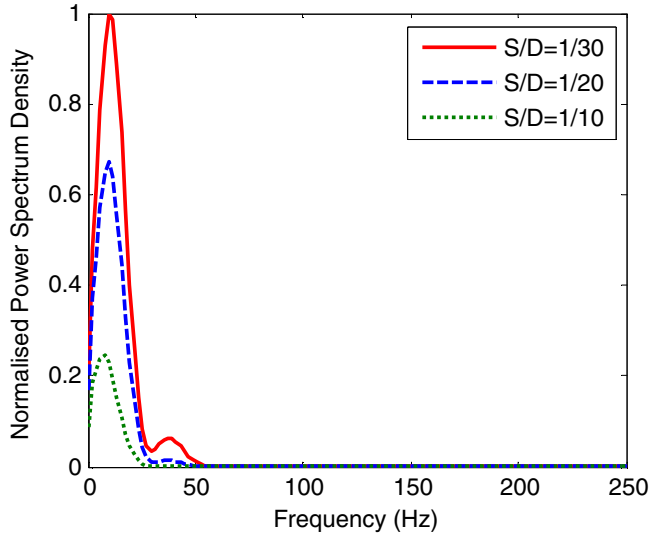**Figure 8.** Frequency characteristics of the electrostatic sensor for variable *S/D*.

Figure 9. Frequency characteristics of the electrostatic sensor for variable *W/D*.

sensitivity distribution on the *z*-axis increases accordingly with the length of the electrode. However, the overall spatial sensitivity remains unchanged at 80%, suggesting that the change in *L* has little impact on the sensitivity. A longer electrode only elongates the sensing area of the sensor along the *z*-axis.

From figures 5–7, we can see a common characteristic that the maximum sensitivity is always located at $z = 0$ and $\theta = \pi/2$ (figure 3), as it is the nearest position on the circular trajectory to the electrode. Figures 5–7 indicate that the sensitivity reduces with the absolute value of *z*. In general, the shorter distance between the electrode and the rotor surface and the larger geometric dimension yield wider and stronger distribution of the spatial sensitivity.

3.2. Spatial filtering effect

3.2.1. Frequency response. As shown schematically in figure 4, W_e is defined as spatial filtering length [9] of the electrostatic sensor. φ_e is the central angle taken by the rotor passing through W_e. τ is the time corresponding to the two peaks of the impulse response with reference to the origin and τ_e is the time difference between the two peaks, which can be expressed by

$$\tau_e = 2\tau = \frac{\varphi_e}{\omega} \tag{13}$$

The frequency response of the sensing system can be determined from the power spectrum $S_h(f)$ of the impulse response $h_s(t)$.

$$S_h(f) = \int_{-\infty}^{+\infty} R_{hh}(\tau)\, e^{-j2\pi f\tau}\, \mathrm{d}\tau \tag{14}$$

where $R_{hh}(\tau) = \int_{-\infty}^{+\infty} h_s(t)\, h_s(t+\tau)\, \mathrm{d}t$ represents the autocorrelation function of $h_s(t)$. Figures 8 and 9 show the power spectral density of the sensing system for variable *S/D* and *W/D*, respectively. It is clear that the electrostatic sensor acts as a low-pass filter in the measurement system. The effective cut-off frequency of the sensor is given by
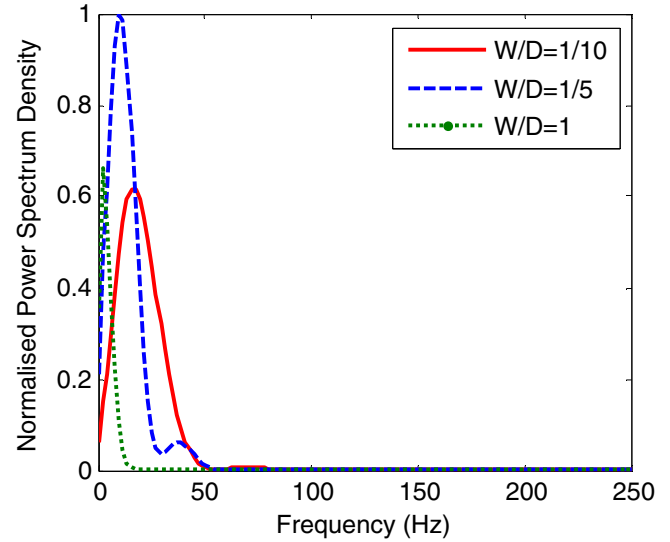
$$f_c = \frac{1}{\tau_e} = \frac{\omega}{\varphi_e} \tag{15}$$

The effect of the distance (*S*) between the electrode and the rotor surface on the frequency response of the sensing system is obtained for $\delta_W = 1/5$, $\delta_L = 1$, $\delta_z = 0$ and $\omega = 10\,\mathrm{rad\,s^{-1}}$ (i.e. 96 rpm). Figure 8 indicates that the amplitude of the frequency response decreases with δ_S. A longer distance between the electrode and the rotor results in less charge on the electrode and hence poorer frequency response and lower power spectral density.

In fact, the length of electrode (*L*) has no influence on the frequency response and bandwidth of the electrostatic sensor because the point charge is rotating at the plane which is perpendicular to the electrode. However, the width of electrode (*W*) plays a more significant part in the frequency response of the sensing system. To investigate this factor, the power spectra for different *W/D* ratios are obtained for $\delta_L = 1$, $\delta_S = 1/30$, $\delta_z = 0$ and $\omega = 10\,\mathrm{rad\,s^{-1}}$ (i.e. 96 rpm), as illustrated in figure 9. The frequency response becomes slower when δ_W increases due to the spatial filtering effect. However, the amplitude response increases initially due to the increased size of the electrode, but declines gradually if the electrode continues to increase in size due to the flat shape of the electrode with reference to the circular motion of the rotor (a wider electrode makes φ_e large and results in poorer frequency response for a given rotational speed).

3.2.2. Spatial filtering length. As shown in figure 4, the spatial filtering length W_e can be determined by

$$W_e = 2\left(S + \frac{D}{2}\right)\tan\frac{\varphi_e}{2} \tag{16}$$

Normalising W_e to *D* yields:

$$\delta_{W_e} = W_e / D = 2\left(\delta_s + \frac{1}{2}\right)\tan\frac{\varphi_e}{2} \tag{17}$$
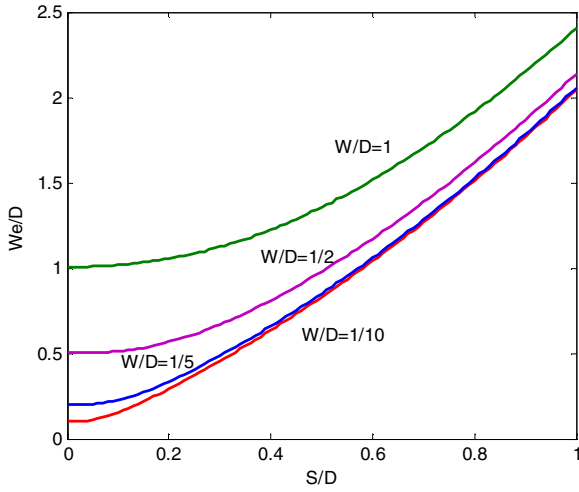
Figure 10. Spatial filtering length of the electrostatic sensor for variable *S/D*.

Equation (17) indicates that W_e has a close relationship with δ_s and φ_e. Moreover, as an indicator of frequency characteristics of the electrostatic sensor, φ_e is mainly affected by the width of the electrode W from the above analysis. To make sense of its influence on the spatial filtering length, W_e is calculated by equations (15) and (17) under the condition that Z equal 0 and δ_S and δ_W are variable. Figure 10 shows W_e increases with the distance between the electrode and the rotor surface. It is worth mentioning that a wider electrode yields a higher φ_e and thus a larger W_e.

3.2.3. Bandwidth. By substituting equation (16) with equation (14), the cut-off frequency of the sensor can be re-written as

$$f_c = \frac{\omega}{2\arctan(\delta_{W_e}/(2\delta_S + 1))} \qquad (18)$$

It can be seen from figure 10 that the minimum value of W_e is always equal to the width of the electrode (*W*), regardless of the rotor diameter *D*. The highest frequency of the signal from the sensor is therefore given by

$$f_{max} = \frac{\omega}{2\arctan(\delta_W/(2\delta_S + 1))} \qquad (19)$$

In practice, the bandwidth of the signal depends on a number of factors, including the random distribution of charges on the rotor surface, the surface roughness and the actual rotational speed. By taking these factors into consideration, the effective signal bandwidth can be defined as

$$B = \frac{K\omega}{2\arctan(\delta_W/(2\delta_S + 1))} \qquad (20)$$

where *K* is a proportionality coefficient, which represents all the factors that affect the bandwidth of the signal. For the single point charge model (figure 2(*b*)), $K = 1$ and *B* is determined by the angular speed, the width of the electrode and the distance between the electrode and the rotor surface. Figure 11 illustrates the effect of δ_W on the bandwidth of the sensor. It is clear that a larger *W/D* ratio yields a narrower bandwidth. However, as expected, *S* has very little effect on the signal bandwidth.
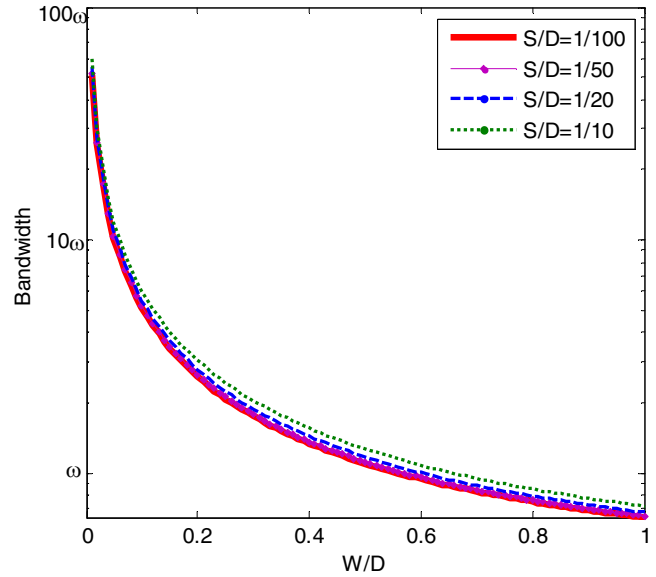

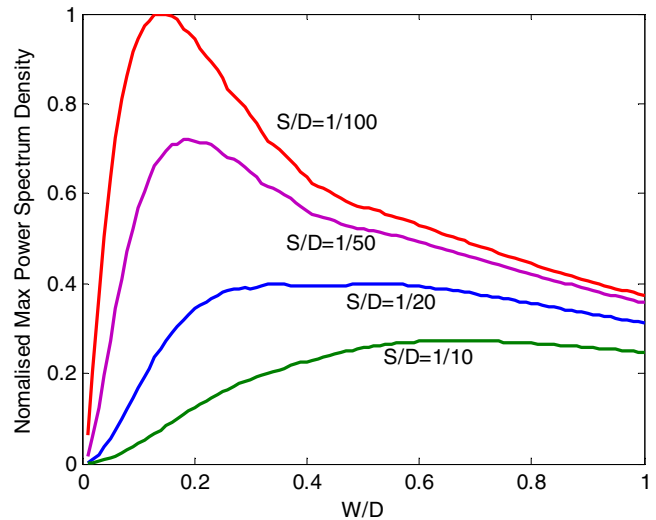**Figure 11.** Bandwidth for variable *W/D*.

Figure 12. Maximum power spectral density for variable *W/D*.

3.3. Optimal width of the electrode

The rotational speed measurement system is based on electrostatic sensing and correlation signal processing, so the sensors should have high spatial sensitivity and wide signal bandwidth for the best system performance in terms of accuracy, repeatability, sensitivity and rangeability [10]. The width of the electrode (*W*) is a crucial parameter that affects the performance of the measurement system and should therefore be optimised with the aid of the modelling results. The above analysis suggests that a wider electrode gives a higher sensitivity but a lower signal bandwidth, implying that a trade-off has to be reached in deciding the optimal width of the electrode. Figure 12 shows the maximum power spectral density for variable *W/D*. It is clear that there is a certain value of *W/D* corresponding to the maximum power spectral density for a given distance between the rotor surface and the electrode. As the distance increases, the power spectral density presents
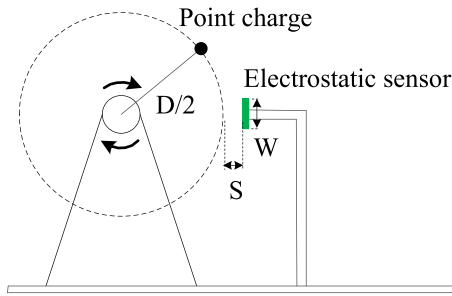
Figure 13. Schematic diagram of the test rig.

Table 1. Test programme.

Test	Material of the point particle	Charge polarity	L (mm)	W (mm)	S (mm)	n (rpm)
1	PF	+	20	3	2	100
2	PVC	−	20	3	2	100, 200
3	PVC	−	20	1, 3	2	100

a declining trend. In consideration of the effects of *W/D* on the spatial sensitivity, signal bandwidth and power spectral density of the sensor (figure 6, figure 11 and figure 12), the optimal width of the electrode is suggested to be between 0.05 D and 0.1 *D*.

4. Experimental validation

4.1. Test rig

Verification tests for the mathematical modelling were conducted on the test rig shown in figure 13. To simulate a point charge in rotational motion, a charged particle with a diameter of 1 mm was fixed on one end of a thin dielectric stick (diameter of the cross-sectional area is less than 1 mm) and the other end of the stick was connected to a rotor which can be rotated at a given rotational speed (*n*). The distance (*D*) between the particle and the centre of the rotor was set to 30 mm to ensure the diameter of the circular trajectory of the charged particle was 60 mm. An electrostatic sensor with a copper-made strip electrode was mounted on the right-hand side of the rotor (figure 13). The shortest distance (*S*) between the electrode and the circular trajectory of the charged particle was 2 mm.

A set of tests as summarized in table 1 were conducted to verify the modelling results. Two particles made of polyurethane foam (PF) and polyvinyl chloride (PVC) were tested. The PF particle carried positive charge in advance, while the PVC particle carried negative charge. To verify the effect of the rotational speed (*n*) and the width (*W*) of the electrode on the sensing characteristics of the sensor, the experiments were undertaken for different rotational speeds (100 rpm and 200 rpm) and different *W* (1 mm and 3 mm). Table 1 summarises the structure parameters of the measurement system, i.e. $\delta_W = 1/60$ or $1/20$, $\delta_L = 1/3$, $\delta_S = 1/30$ and $\delta_Z = 0$.

The current output from the sensing unit was connected to a signal conditioning unit for amplification and filtering. The
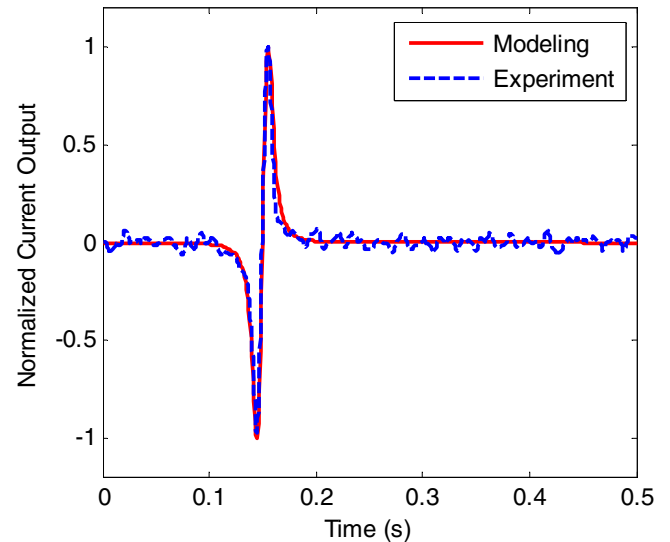

Figure 14. Current output of the sensor for a positively charged particle (*n* = 100 rpm).

signal conditioning unit was designed and constructed so that the signal of interest was not distorted in any way. The cut-off frequency of the low-pass filter in the signal conditioning unit was 1 kHz. The signal was sampled by a data acquisition device at a sampling rate of 4096 Hz. The number of data processed in each record was 2048.

4.2. Experimental results in comparison with modelling data

When a charged particle is in a rotational motion, the induced charge of opposite polarity can be sensed by the electrostatic sensor. The sensor will produce a continuous and periodic current pulse due to the rotational motion. For the purpose of direct comparisons between the modelling data and experimental results, the output signal *S(t)* from the sensor is normalized as follows:

$$S'(t) = \frac{S(t) - \overline{S}}{S_{max} - \overline{S}} \tag{21}$$

where $S'(t)$ is the normalised signal and $\overline{S}$ and S_{max} are the mean and maximum values of *S(t)*, respectively.

Figure 14 shows a typical normalized current output of the sensor when a PF particle with positive charge was rotating at a speed of 100 rpm. It is clear that the experimental response to the single particle movement agrees well with the modelling data, except the experimental waveform contains slight noise. Through the integration of the current output, the induced charge is obtained and plotted in figure 15. As expected, the induced charge is negative, which corresponds to the theory of electrostatic induction.

Figure 16 shows a direct comparison between the simulated and experimental current outputs of the sensor for a negative charged particle. The shape of the current impulse is opposite to that shown in figure 14 due to the oppositely charged particle occurring in the sensing area. In this case, the particle was rotating at a speed of 100 rpm, resulting in only one pulse in the period of 0.5 s. When the speed increased to
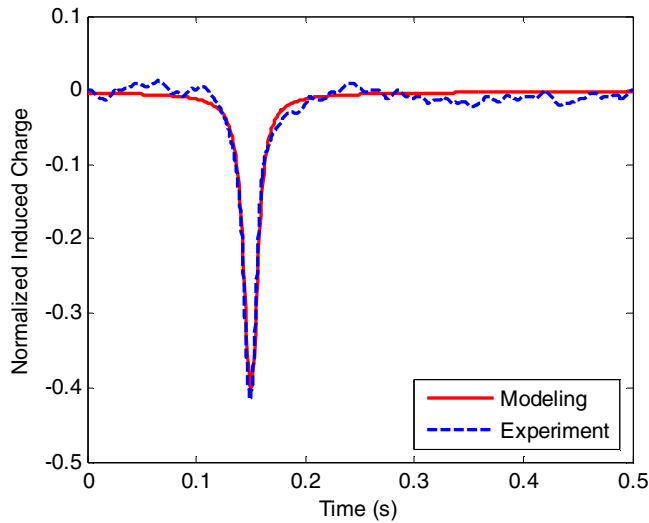
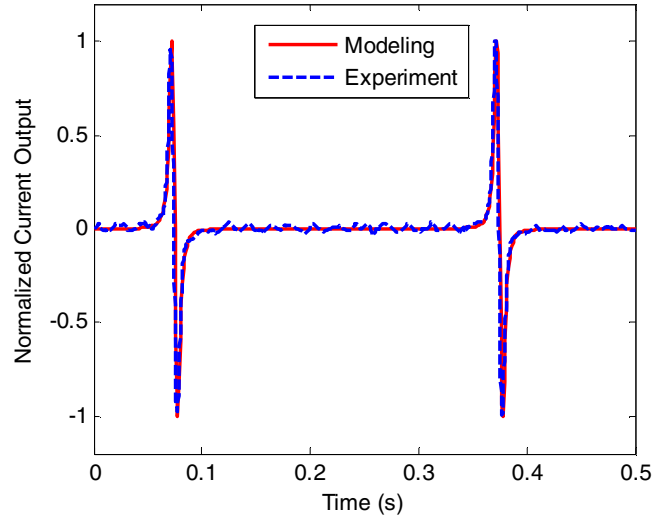**Figure 15.** Induced charge on the electrode for a positively charged particle ($n = 100$ rpm).

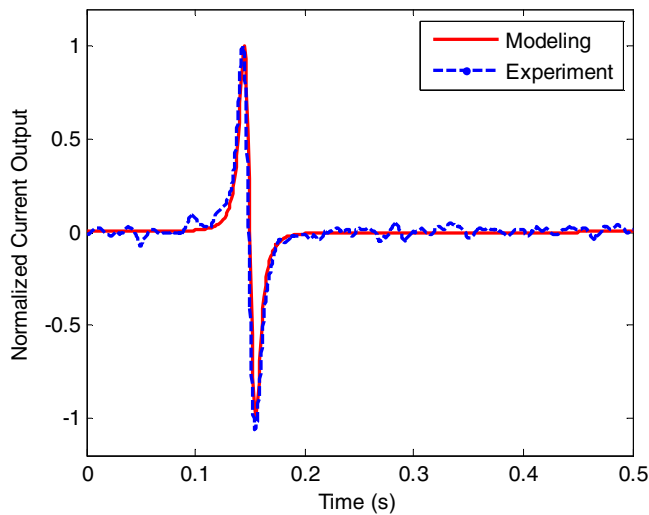**Figure 16.** Current output of the sensor for a negatively charged particle ($n = 100$ rpm).

Figure 17. Current output of the sensor for a negatively charged particle ($n = 200$ rpm).

Figure 18. Current output of the sensor for $W/D = 1/20$ and $W/D = 1/60$.

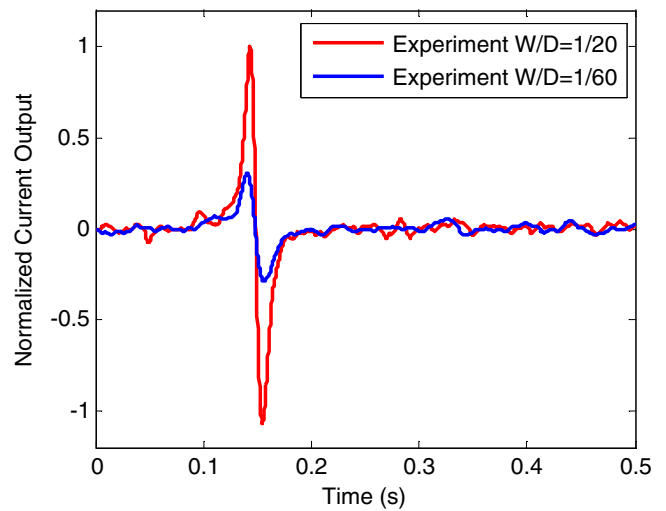**Figure 19.** Frequency characteristics of the sensor for $W/D = 1/20$ and $W/D = 1/60$.

200 rpm, as shown in figure 17, there are two (but narrower) pulses in the same period. The time between the two adjacent pulses is equal to the time taken by the particle rotating for one revolution.

To verify the effect of W on the sensing characteristics of the sensor, two electrodes of different widths (1 mm and 3 mm) were tested for a negatively charged particle rotating at the speed of 100 rpm. It is evident from figure 18 that the wide electrode is more sensitive than the narrow one, just as described in section 3.1. The normalized power spectral density of the experimental signals in comparison with the modelling results is presented in figure 19. The experimental results confirm that a narrower electrode gives a weaker signal but a wider frequency bandwidth, as discussed in section 3.2.1. Figure 19 shows that, unlike those obtained from the computational modelling, the power spectra obtained under experimental conditions contain noise in the higher frequency range (> 100 Hz) due to the limitations of the signal conditioning and processing unit.

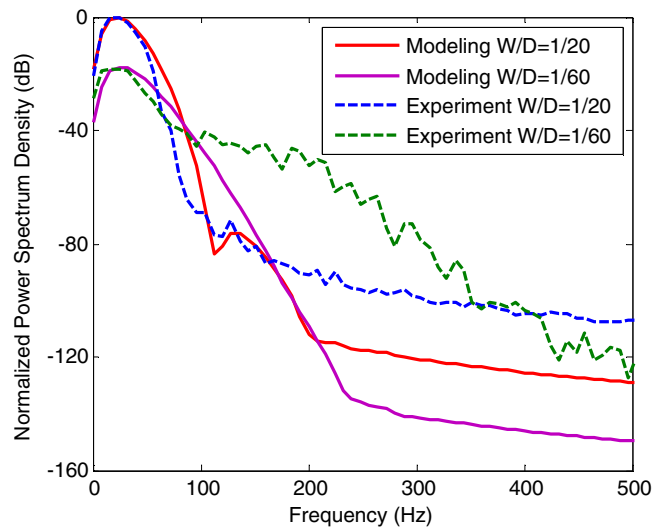## *4.3. Optimised design and installation of the electrostatic sensor*

Through the above comparisons between the experimental results and modelling data, the validity of the models of the strip electrostatic sensor for rotational speed measurement is verified. Moreover, based on the modelling of the sensing characteristics of the sensor, the effects of the physical parameters of the sensor on the system performance and subsequent optimization of the sensor design are achieved. The developed mathematical model (equations (11), (13) and (19)) can be used to obtain optimised sensor design. For a given sized rotor (*D*), the following key parameters are recommended in consideration of the above analysis and practicalities:

 (a) A wider electrode yields higher sensitivity but narrower bandwidth. Thus the optimised width of the electrode (*W*) is suggested in the range of 0.05*D* to 0.1*D* to keep wide signal bandwidth, high power spectral density and relatively high sensitivity simultaneously.
 (b) The length of the electrode (*L*) is not critical, but should normally be in the range of 20 mm to 50 mm in view of the practically suitable physical dimensions of the printed circuit board.
 (c) The distance between the electrode and the rotor surface (*S*) should be between 2 mm to 10 mm. In general, the smaller the size of the rotor, the closer the electrode to the rotor surface. However, it must be borne in mind that *S* should be greater than the minimum safe distance in order to avoid potential direct contact of the electrodes with the rotor.

5. Conclusions

Mathematical models of the strip electrostatic sensors for rotational speed measurement have been established. Based on the models, the sensing characteristics of the sensor, including spatial sensitivity, spatial filtering length and signal bandwidth, have been studied in this paper. Effects of the geometric dimensions of the electrode, the distance between the electrode and the rotor surface, and the rotational speed to be measured on the performance of the sensor have been analyzed. To verify the modelling results, a set of validation experiments were conducted on a purpose-built test rig. The close agreement between the experimental results and the modelling data has verified the validity of the modelling work.

Through the analysis of the modelling results, the optimal dimensions of the electrostatic sensors have been suggested in terms of higher power spectral density, wider bandwidth and higher spatial sensitivity. The optimal width of the electrode should be in the range of 0.05 to 0.1 of the rotor diameter to ensure wide signal bandwidth, high power spectral density and relatively high sensitivity of the sensor. The length of the electrode should normally be in the range of 20 mm to 50 mm, depending on the size of the electronic signal conditioning board. The distance between the electrode and the rotor surface should be between 2 mm to 10 mm.

References

 [1] Wang L, Yan Y, Hu Y and Qian X 2014 Rotational speed measurement through electrostatic sensing and correlation signal processing *IEEE Trans. Instrum. Meas.* **63** 1190–9
 [2] Wang L, Yan Y, Hu Y and Qian X 2013 Rotational speed measurement using electrostatic sensors with single or double electrodes *Proc. IET Conf. on Renewable Power Generation* (*Beijing, China, 9–11, September 2013*) A12
 [3] Wang L, Yan Y, Hu Y and Qian X 2014 Performance assessment of the rotational speed measurement system based on a single electrostatic sensor *Proc. IEEE Int. Instrumentation and Measurement Technology Conf.* (*Montevideo, Uruguay, 12–15 May 2014*) pp 135–8
 [4] Myers R, Islam R, Karmarkar M and Priya S 2007 Magneto electric laminate composite based tachometer for harsh environment applications *Appl. Phys. Lett.* **91** 122904
 [5] Didosyan Y, Hauser H, Wolfmayr H, Nicolics J and Fulmek P 2003 Magneto-optical rotational speed sensor *Sensor Actuators* A **106** 168–171
 [6] Zhang X C, Chen J L, Wang Z T, Zhan N and Wang R C 2012 Digital image correlation using ring template and quadrilateral element for large rotation measurement *Opt. Laser Eng.* **50** 922–8
 [7] Gajewski J 1984 Mathematical model of non-contact measurements of charges while moving *J. Electrostat.* **15** 81–92
 [8] Gajewski J, Glod B and Kala W 1993 Electrostatic method for measuring the two-phase pipe flow parameters *IEEE Trans. Indust. Appl.* **29** 650–5
 [9] Gajewski J 1997 Dynamic effect of charged particles on the measuring probe potential *J. Electrostat.* **40–41** 437–42
[10] Yan Y, Byrne B, Woodhead S and Coulthard J 1995 Velocity measurement of pneumatically conveyed solids using electro dynamic sensors *Meas. Sci. Technol.* **6** 515–37
[11] Murnane S, Barnes R, Woodhead S and Amadi-Echendu J 1996 Electrostatic modelling and measurement of airborne particle concentration *IEEE Trans. Instrum. Meas.* **45** 488–91
[12] Peng L, Zhang Y and Yan Y 2008 Characterization of electrostatic sensors for flow measurement of particulate solids in square-shaped pneumatic conveying pipelines *Sensors Actuators* A **141** 59–67
[13] Krabicka J and Yan Y 2009 Finite-element modeling of electrostatic sensors for the flow measurement of particles in pneumatic pipelines *IEEE Trans. Instrum. Meas.* **58** 2730–6
[14] Shao J, Krabicka J and Yan Y 2010 Velocity measurement of pneumatically conveyed particles using instrusive electrostatic sensors *IEEE Trans. Instrum. Meas.* **59** 1477–84
[15] Xu C, Wang S, Tang G, Yang D and Zhou B 2007 Sensing characteristics of electrostatic inductive sensor for flow parameters measurement of pneumatically conveyed particles *J. Electrostat.* **65** 582–92

[16] Xu C, Li J, Gao H and Wang S 2012 Investigations into sensing characteristics of electrostatic sensor arrays through computational modelling and practical experimentation *J. Electrostat.* **70** 60–71

[17] Zhang J and Coulthard J 2005 Theoretical and experimental studies of the spatial sensitivity of circular electrostatic PF meter *J. Electrostat.* **63** 1133–49

[18] Zhang J, Xu D and Coulthard J 2009 Analysis of characteristics of ring shaped electrostatic meter *Chem. Eng. Commun.* **197** 192–203

[19] Xu C, Wang S and Yan Y 2013 Spatial selectivity of linear electrostatic sensor array for particle velocity measurement *IEEE Trans. Instrum. Meas.* **62** 167–76

[20] Griffiths D J 2012 *Introduction to Electrodynamics* 4th edn (New Jersey: Addison-Wesley)